ELSEVIER

Solid State Ionics 131 (2000) 159–164

SOLID STATE IONICS

www.elsevier.com/locate/ssi

Local and overall ionic conductivity in nanocrystalline CaF_2

W. Puin[a], S. Rodewald[b,*], R. Ramlau[b], P. Heitjans[a], J. Maier[b]

[a]*Institut für Physikalische Chemie und Elektrochemie, Universität Hannover, Callinstraße 3-3A, D-30167 Hannover, Germany*
[b]*Max-Planck-Institut für Festkörperforschung, Heisenbergstraße 1, D-70569 Stuttgart, Germany*

Received 1 January 1999; received in revised form 5 March 1999; accepted 10 March 1999

Abstract

Ionic conductivity data on nanocrystalline CaF_2 is evaluated. The d.c. conductivity is distinctly larger than in coarse-grained materials. The impedance plot exhibits two regimes: a high- and a low-frequency semicircle, the diameters of which increase with increasing grain size. The high-frequency semicircle reflects both bulk transport plus transport along the boundaries while the low-frequency semicircle describes the blocking effect of the grain boundaries. Absolute values and activation energy of the conductivity suggest dominating transport along space charge layers. The increase of the low frequency semicircle is due to increased current constriction because of the appearance of large pores. © 2000 Elsevier Science B.V. All rights reserved.

Keywords: Ionic conductivity; Nanocrystalline; CaF_2

1. Introduction

The consideration of nanocrystalline materials has become very popular recently and many properties, in particular mechanical and electronic properties, have been studied intensively. An overview of studies related to nanocrystalline electroceramics is given in Ref. [1]. Surprisingly, not very much work has been done with respect to ionic or mixed conductors even though ionic transport is intimately related to atomistic aspects [1–3]. An overview on the expected effects is given in [4]. The most obvious one is the enhancement of interfacial contributions due just to the increased density of interfaces. The impact on the overall conductivity may thus stem from the interface core which exhibits a structure different from the grain interior directly or indirectly via space charge effects. In addition the effects of 'edges and corners' will grow correspondingly. If the grain size is of the order of characteristic decay lengths or smaller we have to face mesoscopic effects. One is the change from semi-infinite to finite space charge conditions [5] which means that the space charge distribution of one interface is not decaying to a zero (bulk) value but influenced by one other interface. Also modifications of the ground-state structure in the grain interior must be considered which change the standard term in the chemical potential of the carriers. (Size effects due to delocalisation of the wave

*Corresponding author. Tel.: +49-711-689-1736; fax: +49-711-689-1722.

E-mail address: rodewald@chemix.mpi-stuttgart.mpg.de (S. Rodewald)

0167-2738/00/$ – see front matter
PII: S0167-2738(00)00630-5

functions should be relevant only for proton conductors under very special conditions.)

CaF_2 is well-suited as a model material for such studies, since its macroscopic properties are widely known, it is chemically stable and exhibits well defined grain boundary effects on the ionic conductivity as studied by Saito et al. [6]. Nuclear magnetic resonance (NMR) work on nanocrystalline CaF_2 [7,8] allowed one to differentiate between two F-ion types of distinct diffusivities. The faster ions were ascribed to the grain boundaries, and the slower ones to the grains. The overall diffusivity was found to be considerably enhanced as compared to that in single crystal CaF_2. Similar NMR results were recently obtained for nanocrystalline $LiNbO_3$ [8,9]. The increased diffusivity in nanocrystalline CaF_2 corresponds to the results of conductivity measurements on the same material by impedance spectroscopy [10]. The present contribution is essentially an evaluation of the data in Ref. [10] by using the model developed in Ref. [11] to deconvolute the different conductivity contributions in a polycrystalline sample including space charge phenomena. In addition TEM studies are employed to take proper account of morphological variations.

2. Impedance analysis of micro- and nanocrystalline materials

In general the impedance analysis of polycrystalline materials is complex. The grain boundary network topology can be complicated and, thus, also the percolation behaviour. Different types of grain boundaries can exist in the same material according to type, structure, misfit angle, inclusions (glasses or pores) etc. Additional complications occur if the crystallites are not homogeneous. In the following we assume that the grain boundary effect can be mimicked by a brick layer model with one kind of grain boundary and follow Ref. [11]. It is shown in Ref. [12] that results of the brick-layer model are expected to be a good approximation for this material even if the microstructure deviates substantially from the model. In other words we assume a cubic primitive microstructure consisting of cubic grains (thickness L) separated by identical boundaries. The equivalent circuit then approximately reduces to the

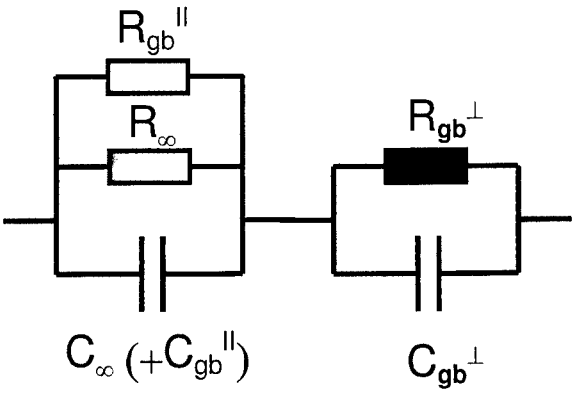

Fig. 1. Equivalent circuit model assuming the different contributions to the impedance spectra in the brick layer approximation. It is assumed that the parallel interfacial pathway is also blocked by $R_{gb}\perp$ [10].

circuit given in Fig. 1. The equivalent circuit in Fig. 1 consists of two parallel circuit-elements which are denoted by resistance and capacitance values in a series circuit. R_∞, C_∞ refer to the bulk, $R_{gb}^{\parallel}$, $C_{gb}^{\parallel}$, and $R_{gb}^{\perp}$, $C_{gb}^{\perp}$ to the boundary values. In terms of the complex conductivities the superposition is given by Eq. (1):

$$\hat{\sigma}_m = \frac{\hat{\sigma}_\infty \hat{\sigma}_L^{\parallel} + \beta_L^{\parallel} \varphi_L \hat{\sigma}_L^{\parallel} \hat{\sigma}_L^{\perp}}{\hat{\sigma}_L^{\perp} + \beta_L^{\perp} \varphi_L \hat{\sigma}_\infty} \tag{1}$$

The total complex conductivity $\hat{\sigma}_m$ has contributions from the complex bulk conductivity $\hat{\sigma}_\infty$ and the interfacial layer parallel and perpendicular complex conductivities $\hat{\sigma}_L^{\parallel}$ and $\hat{\sigma}_L^{\perp}$. Both $\hat{\sigma}^{\perp}$ and $\hat{\sigma}^{\parallel}$ consists of core and space charge effects. A more detailed analysis is given in Ref. [11]. In an impedance plot, the circuit of Fig. 1 should lead to two semicircles. Usually the low frequency semicircle, corresponding to a higher capacitance, reflects the series effect the at grain boundaries, whereas the high frequency semicircle, in which $C^{\parallel}$ is normally negligible compared to C_∞, refers to bulk plus parallel layers. This simple model allows one to take account of the grain boundary anisotropy. The anisotropy may be due to the sandwich structure (space charge region | core | space charge region) and/or to the profile character of the space charge regions themselves (e.g. inversion layers). Thus, in the same material, blocking and short-circuiting behaviour of the grain boundary may

be perceived [11]: The grain boundary can provide fast pathways but can also (in the direction of measurement) act as an obstacle for the transport from grain to grain as indicated in Fig. 1. Also series blocking effects can often simply be traced back to current constrictions due to insufficient contact [13,14]. In this case the measured activation energy roughly corresponds to the bulk value. In the case of highly conducting layers via space charges the activation energy is usually somewhat higher than the migration enthalpy of the enriched defect type. The difference is smaller, the larger the interfacial effect. The effective series and parallel space charge contributions can be derived from the profile [11,15]. In the following we are especially interested in the second contribution. Thus the conductivity of the parallel interfacial layer $\sigma_L^{\parallel}$ [11], [16] to be inserted in Eq. 1 is given by:

$$\sigma_L^{\parallel} \cong \Delta\sigma_L^{\parallel} = u_V F c_{V\infty} \frac{2\vartheta_V}{1-\vartheta_V} \cong u_V F \sqrt{c_{V0} c_{V\infty}}. \quad (2)$$

In the brick layer model the volume fraction of the space charge layers is

$$\varphi_L = 6(2\lambda/L) = \frac{12}{L}\sqrt{\frac{\varepsilon_0 \varepsilon_r RT}{2F^2 c_{V\infty}}} \quad (3)$$

with $\beta_L^{\parallel} = 2/3$. The result is

$$\sigma_{\mathrm{m}}^{\parallel} \cong 4u_V \sqrt{2\varepsilon_r \varepsilon_0 RT c_{V0}}/L. \quad (4)$$

The quantities u_V, $c_{V\infty}$, c_{V0} denote mobility, bulk defect concentration and defect concentration in the first layer adjacent to the interface core of the enhanced carriers (here taken as the vacancy). The enhancement is characterized by the 'degree of influence' (on the vacancies) ϑ_V as defined in Ref. [11]. L is the thickness of the grain, $\beta_L^{\parallel}$ the fraction of interfaces contributing to the conduction.

In nano-crystalline materials the fraction of interfacial regions is much more pronounced and consequently their impact on the overall electrical conductivity is enhanced. In addition, there is the possibility that the Debye-length is comparable or even larger than the crystallite sizes. In these cases, space charge effects may be extremely high, the crystallites may be charged everywhere and no bulk profiles may be attained within the mesoscopic sample [5]. In these cases, it was derived that for large effects [5]:

$$\sigma_{\mathrm{m}}^{\parallel} \cong f u_V \sqrt{2\varepsilon_r \varepsilon_0 RT(c_{V0} - c_V^*)}/L \quad (5)$$

(c_V^*: concentration in the centre). The dependence of c_V^* on c_{V0} and L necessary for an explicit treatment is given in Ref. [5]. To be precise Eq. (5) was derived for nano-sized films with $f=2$. The value $f \cong 4$ should give a first rough estimate for nano-crystalline (cubic) grains, even though for precise considerations the simultaneous influence of all six interfaces should be considered.

3. Experimental

Nanocrystalline powder of CaF_2 (n-CaF_2) with an average particle diameter of 9 nm was prepared by the inert gas condensation method. The impurity level was determined to be $\leq$30 ppm except for Na (400 ppm). Cylindrical pellets (with a density of about 96%) were formed under a pressure of 2 GPa, coated with Ag on both sides and placed between the electrodes of an air tight measurement cell. The impedance of the sample was measured using a HP 4192A impedance analyser from 5 to 13 MHz at temperatures in the range 390–500 K. More details on the preparation and measurement can be found in reference [10]. Transmission Electron Microscopy (TEM) investigations were carried out with a PHILIPS CM30/ST electron microscope operating at 300 kV (point resolution 0.19 nm). The slightly sintered nano-crystalline powder was dispersed in n-butanol and then dropped on a specimen grid which was a perforated carbon film. TEM images were taken in the bright-field mode to determine the grain sizes, and in the high resolution mode to investigate the pore sizes.

4. Results and discussion

The impedance spectra of the freshly prepared samples show three semicircles. These impedance spectra can be interpreted in terms of the equivalent circuit given in (Fig. 1) taking the additional contributions of blocking electrode effects into account.

The semicircle at very low frequencies is caused by electrode polarisation effects and will not be further discussed in this contribution. The two other partly overlapping depressed semicircles can be assigned to bulk and grain boundaries. As discussed above the high frequency contribution can be attributed to the parallel combination of bulk and parallel boundary pathways '‖' while the low frequency semicircle describes the blocking of these pathways by perpendicular boundary effects '⊥' [11]. The resistance obtained from the low-frequency semicircle is about 10 times larger than the resistance of the high-frequency semicircle. Nevertheless the total d.c. contribution is far greater than the pure bulk contribution of coarse grained material. By annealing the sample for 30 min at 505 K the resistance of the low-frequency semicircle increases by almost one order of magnitude, whereas the high-frequency semicircle shows only an increase of a factor of two (Fig. 2).

The very low resistance of the high-frequency semicircle compared to the normally measured bulk resistances (Fig. 3) of CaF_2 may be simply interpreted in terms of space charge effects as the following arguments suggest: Measurements on m-CaF_2 (CaF_2 with grain size in the micron-region) by Saito et al. [6] showed that space charge effects play

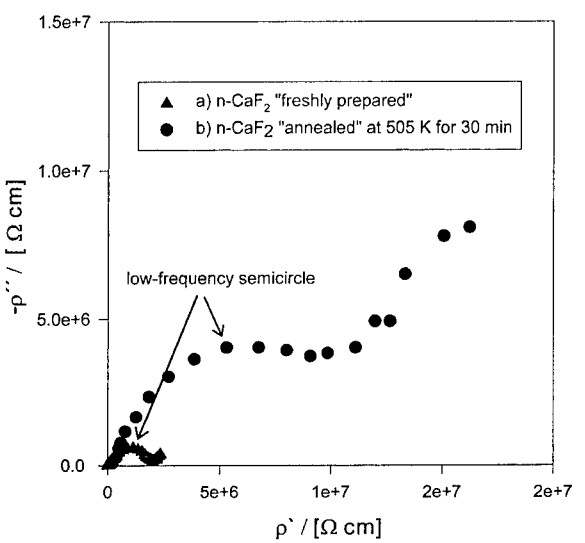

Fig. 2. Impedance spectra for nanocrystalline CaF_2 samples (a) 'freshly prepared' and (b) 'annealed' [9].

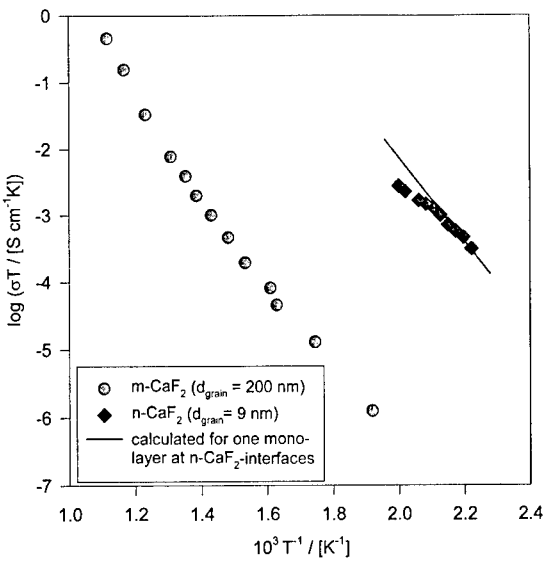

Fig. 3. Temperature dependence of the conductivities of nano- and micro-crystalline CaF_2 derived from the high-frequency semicircles [5,9]. The line represents the estimated conductivities assuming a pronounced space charge effect [5].

a significant role in polycrystalline materials. The space charge potential can be increased by special chemical treatment (heterogeneous doping by SiO_2, contamination by SbF_5 or BF_3). This behaviour is completely analogous to the experiments on Ag-halides (heterogeneous doping by Al_2O_3 [17], contamination with NH_3 or $(CN)_2$ [18]). The solid line indicated in Fig. 3 is obtained simply by scaling up the space charge effects of Saito et al. according to the increased interfacial density. The slope of the line is approximately the activation energy of the vacancies and suggests, accumulation in the grain boundary core. Assuming that the increased vacancy concentration is responsible for the enhancement, the line meets the correct order of magnitude. The systematic deviation at increased temperature is definitely due to sintering and coarsening.

If the grain size of the material becomes smaller than four times the Debye length, even the core of the grains becomes fully charged. In that case, an additional enhancement factor comes into play. As the results show, this 'nano size' effect [5] is obviously not observed here (however see results obtained for $AgI:Al_2O_3$ composite [4]). This is in agreement with the fact that the computed Debye

length (~1 nm) is much below the grain size (~9 nm) owing to the high impurity concentration of Na+-ions.

The second semicircle can be explained in the following way. Both bulk and space charge transport perceive the perpendicular boundaries. This may be due to core effects or due to current constriction. The comparably low capacitance points towards the second effect. It is also supported by the activation energy of 0.8 eV which is close to the bulk value [14]. Increased current constriction is certainly responsible for the fact that the low frequency semicircle increases with temperature. TEM images (Fig. 4) reveal a coarsening of the grains connected with the generation of significant pores causing serious constriction effects [5]. The generation of large pores is understandable since no pressure is applied during the grain growth process.

Therefore two effects, both caused by annealing, have to be considered: (i) The diminishing of the volume fraction of highly conducting parallel pathways (space charge layers) leading to an increase of the resistance of the high-frequency semicircle and (ii) current constriction effects which become more serious due to the formation of large pores. Applying pressure would lead to densification and probably eliminate the second effect. The grain coarsening itself is an inherent problem in nanocrystalline materials due to high interfacial energy. In particular, in ionic conductors this may be an even more serious problem due to facilitated kinetics. A way-out can be the use of nano-composites, e.g. heterogeneous doping of fluorides by silica [19], in which the phase distribution makes grain growth much more difficult.

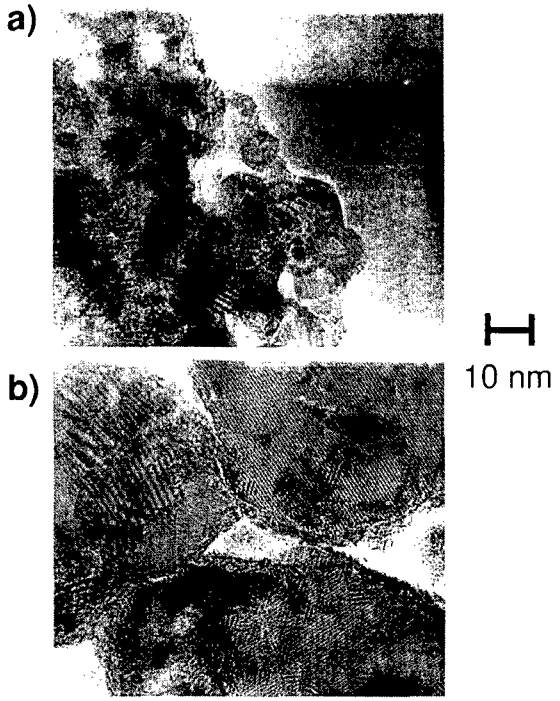

Fig. 4. TEM image of the nano-crystalline CaF_2 powder: (a) The 'freshly prepared' sample exhibits a small grain size and only little pores, (b) The 'annealed' sample (at 870 K for 90 min) shows larger grain sizes (d_{grain} >50 nm) and the formation of large pores.

5. Conclusions

Nanocrystalline CaF_2 shows a significantly higher overall conductivity than the micro-crystalline material. This behaviour can be completely understood in terms of the large fraction of interface regions in the nanocrystalline material. By assuming a pronounced space charge effect (one monolayer of absorbed at the grain boundary interface) the order of magnitude and temperature dependence of the overall conductivity in n-CaF_2 can be explained. The appearance of the mesoscopic space charge effect predicted in Ref. [5] demands the preparation of highly pure n-CaF_2. The significant porosity leads to current constriction.

Acknowledgements

The authors thank the Deutsche Forschungsgemeinschaft and the Fonds der Chemischen Industrie for financial support.

References

[1] Y.-M. Chiang, J. Electroceramics 3 (1997) 205.
[2] H.L. Tuller, J. Electroceramics 3 (1997) 211.
[3] Y.-M. Chiang, E.B. Chiang, I. Lavik, H. Kosacki, H.L. Tuller, J. Electroceramics 1 (1997) 7.
[4] J.-S. Lee, J. Maier, Solid State Ionics 131 (2000).
[5] J. Maier, Solid State Ionics 23 (1987) 59.
[6] Y. Saito, J. Maier, J. Electrochem. Soc. 142 (1995) 3078.

[7] W. Puin, P. Heitjans, W. Dickenscheid, H. Gleiter, in: O. Kanert, J.-M. Spaeth (Eds.), Defects in Insulating Materials, World Scientific, Singapore, 1993, p. 137.
[8] P. Heitjans, A. Schirmer, in: J. Kärger, P. Heitjans, R. Haberlandt (Eds.), Diffusion in Condensed Matter, Vieweg, Wiesbaden, 1998, p. 116.
[9] D. Bork, P. Heitjans, J. Phys. Chem. B 102 (1998) 7303.
[10] W. Puin, P. Heitjans, NanoStructured Mater. 6 (1995) 885.
[11] J. Maier, Ber. Bunsenges. Phys. Chem. 90 (1986) 26.
[12] J. Fleig, J. Maier, J. Electrochem. Soc. 145 (1998) 2081.
[13] J.E. Bauerle, J. Phys. Chem. Solids 30 (1969) 2657.
[14] J. Fleig, J. Maier, in this issue
[15] J. Maier, Prog. Solid State Chem. 23 (1995) 171.
[16] J. Maier, J. Electrochem. Soc. 134 (1987) 1524.
[17] J. Maier, S. Prill, B. Reichert, Solid State Ionics 28–30 (1988) 1465.
[18] U. Lauer, J. Maier, Sensors and Actuators B2 (1990) 125.
[19] K. Hariharan, J. Maier, J. Electrochem. Soc. 142 (1995) 3469.